



Universiteit
Leiden
The Netherlands

Investigating 3R in vivo approaches for bio-distribution and efficacy evaluation of nucleic acid nanocarriers: studies on peptide-mimicking ionizable lipid

Giselbrecht, J.; Pinnapireddy, S.R.; Alioglu, F.; Sami, H.; Sedding, D.; Erdmann, F.; ... ; Wolk, C.

Citation

Giselbrecht, J., Pinnapireddy, S. R., Alioglu, F., Sami, H., Sedding, D., Erdmann, F., ... Wolk, C. (2022). Investigating 3R in vivo approaches for bio-distribution and efficacy evaluation of nucleic acid nanocarriers: studies on peptide-mimicking ionizable lipid. *Small*, 18(18). doi:10.1002/sml.202107768

Version: Publisher's Version

License: [Creative Commons CC BY-NC-ND 4.0 license](https://creativecommons.org/licenses/by-nc-nd/4.0/)

Downloaded from: <https://hdl.handle.net/1887/3484732>

Note: To cite this publication please use the final published version (if applicable).

Investigating 3R In Vivo Approaches for Bio-Distribution and Efficacy Evaluation of Nucleic Acid Nanocarriers: Studies on Peptide-Mimicking Ionizable Lipid

Julia Giselbrecht, Shashank Reddy Pinnapireddy, Fatih Alioglu, Haider Sami, Daniel Sedding, Frank Erdmann, Christopher Janich, Michaela Schulz-Siegmund, Manfred Ogris, Udo Bakowsky, Andreas Langner, Jeroen Bussmann,* and Christian Wölk*

Formulations based on ionizable amino-lipids have been put into focus as nucleic acid delivery systems. Recently, the in vitro efficacy of the lipid formulation OH4:DOPE has been explored. However, in vitro performance of nanomedicines cannot correctly predict in vivo efficacy, thereby considerably limiting pre-clinical translation. This is further exacerbated by limited access to mammalian models. The present work proposes to close this gap by investigating in vivo nucleic acid delivery within simpler models, but which still offers physiologically complex environments and also adheres to the 3R guidelines (replace/reduce/refine) to improve animal experiments. The efficacy of OH4:DOPE as a delivery system for nucleic acids is demonstrated using in vivo approaches. It is shown that the formulation is able to transfect complex tissues using the chicken chorioallantoic membrane model. The efficacy of DNA and mRNA lipoplexes is tested extensively in the zebra fish (*Danio rerio*) embryo which allows the screening of biodistribution and transfection efficiency. Effective transfection of blood vessel endothelial cells is seen, especially in the endocardium. Both model systems allow an efficacy screening according to the 3R guidelines bypassing the in vitro–in vivo gap. Pilot studies in mice are performed to correlate the efficacy of in vivo transfection.


1. Introduction

The therapeutic and prophylactic power of nucleic acids has become clinically relevant in the last decade, with several formulations now approved for clinical use.^[1] Furthermore, DNA- or RNA-based vaccines were the first approved vaccines in the current severe acute respiratory syndrome coronavirus type 2 pandemic, namely Sputnik V (Gamaleya Research Institute), Comirnaty (Biontech/Pfizer), Spikevax (Moderna), Vaxzevria (Astra Zeneca), and Ad26.COVS.2 (Johnson & Johnson). The major hurdle for nucleic acid delivery systems is protection of the genetic cargo against degradation and thereby achieving efficient delivery into the target cells. Two main groups of nucleic acid delivery systems for systemic administration are known: i) Viral vectors which are highly efficient due to

J. Giselbrecht, F. Erdmann, C. Janich,^[†] A. Langner
Department of Medicinal Chemistry/Department of Pharmacology
Institute of Pharmacy Martin Luther University Halle-Wittenberg
Wolfgang-Langenbeck-Str. 4, 06120 Halle (Saale), Germany

S. R. Pinnapireddy, U. Bakowsky
Department of Pharmaceutics and Biopharmaceutics
University of Marburg
Robert-Koch-Str. 4, 35037 Marburg, Germany

S. R. Pinnapireddy
CSL Behring Innovation GmbH
Emil-von-Behring-Str. 76, 35041 Marburg, Germany

 The ORCID identification number(s) for the author(s) of this article can be found under <https://doi.org/10.1002/smll.202107768>.

© 2022 The Authors. Small published by Wiley-VCH GmbH. This is an open access article under the terms of the Creative Commons Attribution-NonCommercial-NoDerivs License, which permits use and distribution in any medium, provided the original work is properly cited, the use is non-commercial and no modifications or adaptations are made.

^[†]Present address: Federal Office of Consumer Protection and Food Safety, Department 3: Veterinary Drugs, Berlin, Germany

F. Alioglu, H. Sami, M. Ogris
Faculty of Life Sciences
Department of Pharmaceutical Sciences, Laboratory
of Macromolecular Cancer Therapeutics (MMCT)
University of Vienna
Althanstrasse 14, Vienna 1090, Austria

D. Sedding
Internal Medicine III
Medical Faculty of Martin Luther University Halle-Wittenberg
Ernst-Grube-Str. 40, 06120 Halle (Saale), Germany

M. Schulz-Siegmund, C. Wölk
Pharmaceutical Technology
Medical Faculty
University Leipzig
Eilenburger Straße 15a, 04317 Leipzig, Germany
E-mail: christian.woelk@pharmazie.uni-halle.de

J. Bussmann
Division of BioTherapeutics, Leiden Academic Center for Drug Research
Leiden University
Einsteinweg 55, Leiden 2333 CC, The Netherlands
E-mail: j.bussmann@lacdr.leidenuniv.nl

DOI: 10.1002/smll.202107768

evolutionary acquired molecular biological mechanisms, but which are also associated with several drawbacks (e.g., insertional oncogenesis, excessive immune reactions).^[2] ii) Non-viral delivery systems, including inorganic or organic compounds, which complex/adsorb nucleic acids and deliver it to the target tissue by utilization of physiological transport processes or physical triggers (e.g., magnetic fields, pressure).^[3]

Among the non-viral delivery systems, cationic or ionizable lipids are the most advanced nucleic acid delivery platform. Due to positive charges these lipids complex nucleic acids and assemble into structures termed as lipoplexes or also nucleic acid–lipid nanoparticles.^[4] Lipoplex is a general term for nucleic acid/cationic lipid complexes of various nano-scaled structures. Since pioneer research of Felgner,^[5] several classes of effective cationic lipid formulations, including lipids with ionizable amino functions, suitable as transfection reagents have been established.^[6] Multivalent ionizable lipids are a prominent class of lipids for nucleic acid delivery due to the efficient DNA encapsulation mediated by the head group. Several representatives have been developed. The group around Safinya developed dendritic ionizable lipids,^[7] which are commercially available from Avanti Polar Lipids (No. 890000—MVL5). Also 2,3-dioleoyloxy-*N*-[2(sperminecarboxamido)ethyl]-*N,N*-dimethyl-1-propaniminium trifluoroacetate, the key lipid of the Lipofectamine-series distributed by ThermoFisher Scientific, belongs to this group of lipids. An exhaustive list of such multivalent cationic lipids has been summarized in reviews.^[8] A promising class of ionizable multivalent cationic lipids developed in our lab based on malonic acid amides.^[9] The second generation of these malonic acid diamides, a lipid species with a peptide-mimicking backbone,^[10,11] showed high efficiency in cell culture models. Nevertheless, the behavior of non-viral nucleic acid delivery systems under physiological conditions is a key step in the development of efficient formulations. The complex environment of organisms is difficult to mimic in vitro experiments. Though, there exists a gap between in vitro performance and in vivo efficacy. To close such a gap and study lipoplex formulations in living organisms, test strategies in accordance with the 3R guidelines are a promising way. The 3R guidelines take care for a greater responsibility in research/experiments with animal models based on the replacement reduction and refinement of animal experiments.^[12] Such 3R models with expressiveness for in vivo behavior are needed for first-time evaluation under in vivo conditions bypassing expensive and time-consuming experiments with mammals, which are also connected with time-consuming permission processes. The chorioallantoic membrane model of

the fertilized chicken egg and the study of zebrafish embryos represent a practicable intermediate step to rodent experiments for nucleic acid transfer studies.

The chick embryo chorioallantoic membrane (CAM) is a multifaceted experimental model with in vivo quality which can be used for drug delivery and toxicology studies.^[13] Recent studies demonstrate that the CAM is also an effective model to test non-viral nucleic acid delivery systems in complex tissues.^[13–18]

Experiments with zebrafish larvae can be performed within high-throughput screening setups and thus become very promising for nanomedicine research.^[19] Key factors for nanomedicine research are transparent zebrafish larvae, fluorescent reporter lines, and sophisticated imaging techniques (confocal or light sheet microscopy). The fact that at the genomic level, 76% of human genes (82% of disease related genes) have orthologues in zebrafish (compared to 84% in mice), and that many relevant physiological homologies exist make zebrafish an efficient tool to evaluate in vivo behavior of nanoparticles.^[19,20] There are several studies performed: toxicity and biodistribution screenings, nanoparticle based protein delivery or cancer therapy.^[19] Despite the high potential of this in vivo model system, it is rarely used in studying the efficacy of nanomedicines loaded with nucleic acids.^[21,22] The present article contributes toward closing this gap by demonstrating the applicability of the zebrafish embryo model to study pharmacokinetic and pharmacodynamics aspects of non-viral nucleic acid delivery on selected lipid formulations.

OH4:DOPE 1:1 (*n:n*) is an ionizable multivalent cationic liposome formulation that efficiently complexes nucleic acids (**Figure 1**, referred to OH4:DOPE). Detailed characterization of this complex formation process between the lipid mixture and plasmid DNA (pDNA) as well as stability evaluation of the resulting lipoplexes were published previously.^[23,24] The efficient in vitro DNA transfer of OH4:DOPE lipoplexes was demonstrated for various cell lines: A549 (adenocarcinomic human alveolar basal epithelial cells), HELA (human cervical cancer cells), LLC-PK1 (porcine renal tubular epithelial cells), HEK 293T (human embryonic kidney cells), and C2C12 (mouse myoblast cell line).^[18,23–26] These studies also demonstrate that the most efficient loading degree of lipoplexes can be obtained at an N/P ratio (ratio of primary amines of the lipid formulation to phosphate moieties of DNA, the representative ratio for loading degree) of 4. Nevertheless, currently no information exists, on how the formulation behaves in vivo, despite this information is needed to figure out a clinical application.

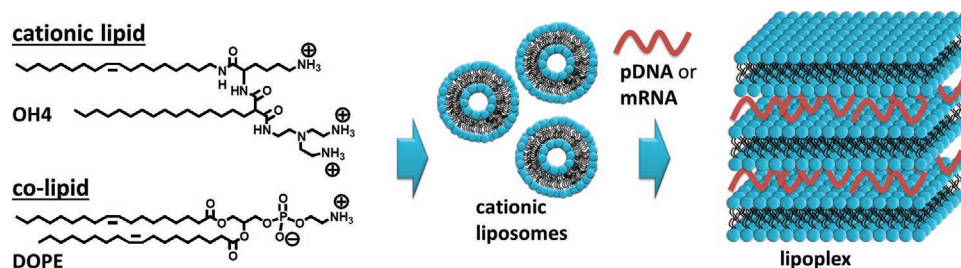


Figure 1. Structure of lipid components, which are used in an equimolar ratio to build cationic liposomes. The interaction of cationic liposomes with nucleic acids results in the assembly to lipoplexes (nucleic acid/lipid complexes).

The main focus of this article is proof-of-efficacy studies using in vivo approaches, in order to investigate the behavior of OH:DOPE lipoplexes after systemic administration. To achieve this goal we explored the potential of simpler in vivo models (according to 3 R guidelines of replacement, reduction and refinement of animal experiments), the above mentioned CAM model and zebrafish larvae model. Both model systems prove efficacy of the lipid formulation regarding successful nucleic acid transfer in comparison to the commercially available lipofectamine 2000. The investigations demonstrate the power of the zebrafish larvae to get pharmacokinetic/biopharmaceutical information as well as pharmacodynamics data in a highly efficient way with high numbers of treated animals. Finally, first in vivo experiments in mice will be used to build a bridge between these two in vivo models according to 3R (CAM, zebrafish embryo) and mammalian models. This strategy can offer correlating the performance of these models with rodent data for investigating their performance as accepted preclinical in vivo test systems for gene therapeutics. The presented experiments also identified target cells/tissues which were efficiently transfected with OH4:DOPE lipoplexes. Therewith the article paves the way for the development of clinical applications.

2. Results and Discussion

2.1. Particle Size Measurements

OH4:DOPE was formulated in 10 mM MES-buffer pH 6.5 to small vesicles with a z-average diameter of ≈ 128 nm and a particle size distribution illustrated by a PDI of 0.369 (Table 1). This is an acceptable distribution taking into account that extrusion of the liposomes was avoided due to adsorption effects of lipids at the extruder membrane. The PDI value can be explained by the bimodal size distribution (mode 1 ≈ 80 nm, mode 2 ≈ 200 nm, Figure S1, Supporting Information). The cationic character, which is needed for efficient nucleic acid encapsulation, is demonstrated by a ζ potential of ≈ 91 mV. After mixing the cationic liposomes with a negatively charged nucleic acid (mRNA or pDNA), spontaneous formation of lipid/nucleic acid-complexes (lipoplexes) occurs. The incubation of OH4:DOPE liposomes with pDNA-GFP (3.5 kbp) results in lipoplexes with a z-average diameter of

≈ 214 nm (PDI = 0.331) and a ζ potential of ≈ 62 mV (Table 1). This size is in agreement with previous studies using a larger plasmid (4.7 kbp) while the zeta potential in the present study is higher compared to the lipoplexes prepared from 4.7 kbp plasmids.^[24,26] OH4:DOPE mRNA-GFP (1 kb) lipoplexes were also examined. Compared to DNA lipoplexes, the particle size increases slightly to 243 nm and the distribution gets slightly broader (Table 1; Figure S1, Supporting Information). The zeta ζ potential is reduced to ≈ 51 mV (see Table 1). For lipoplex tracking analysis Rho-DOPE is a suitable fluorescence probe.^[18,25,27] The effect of 0.5 mol% Rho-DOPE on the lipoplex size and charge was screened, because we used the labelled lipoplexes in the zebrafish experiments. The addition of the fluorescence label had a negligible effect on the size of liposomes or lipoplexes (Table 1; Figure S1, Supporting Information). Nevertheless, the incorporation of the Rho-DOPE label into liposomes or lipoplexes decreases the ζ potential (Table 1). Still, the values remain highly positive.

Before administration to the in vivo test systems, additional biocompatibility tests were performed. The stability of OH4:DOPE pDNA-GFP lipoplexes in presence of either DNase or polyanions, a model for the extracellular matrix, was already evaluated by us in Janich et al.^[24]. So for the present investigation, we focused on the particle size stability of the OH4:DOPE pDNA-GFP lipoplexes in 10% v/v sterile filtered human serum at 37 °C for 18 h. Size stability testing of nanoparticles is an important preclinical parameter before systemic administration in order to screen for the risk of particle aggregation in blood, to test for the risk of embolism events.^[28]

We have chosen time dependent DLS measurements with focus on the correlation function, due to the high particle number of serum components. This method is comparable to turbidimetric measurements. If severe aggregation occurs, a shift of the entire curve to increased time values and a prominent noisy background after the continuous decay of the correlation function would appear.^[29] Figure 2 demonstrates no pronounced changes during the incubation time, which indicates the absence of flocculation and precipitation processes. The calculation of the size distribution from the correlation functions showed no critical increase in particle size (Figure S2, Supporting Information). Therefore, size stability in the physiological environment of blood serum can be assumed. The later described in vivo experiments in all three model systems support this assumption. Flocculation and sedimentation

Table 1. Particle size in z-average diameter (d) and polydispersity index (PDI) (both parameters calculated by cumulant analysis of dynamic light scattering (DLS) data) as well as ζ -potential of liposome and lipoplex formulations used in this work. The values are given as mean \pm standard deviation, $n = 3$. Representative correlation functions as well as the distribution curves are shown in Figure S1, Supporting Information.

OH4:DOPE N/P 4 without fluorescence label			
	ζ -potential [mV]	d [nm]	PDI
liposomes	91.0 ± 3.0	127.7 ± 1.0	0.369
lipoplexes pDNA-GFP	61.7 ± 2.5	213.7 ± 1.1	0.331
lipoplexes mRNA-GFP	51.4 ± 0.6	243.0 ± 1.7	0.433
OH4:DOPE + 0.5 mol% Rho-DOPE N/P 4			
	ζ -potential [mV]	d [nm]	PDI
liposomes	75.4 ± 2.7	108.2 ± 0.4	0.306
lipoplexes pDNA-GFP	47.9 ± 0.6	213.0 ± 2.2	0.277
lipoplexes mRNA-GFP	46.6 ± 1.3	214.7 ± 1.3	0.285

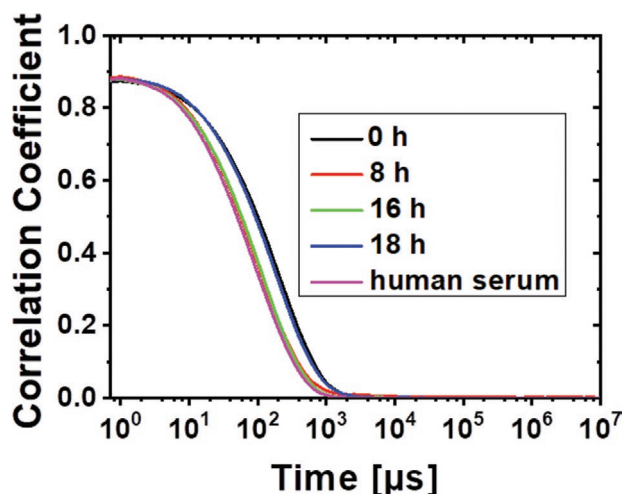


Figure 2. Autocorrelation functions of OH4:DOPE pDNA-GFP lipoplexes in MES-buffer pH 6.5 with 10% sterile filtered human serum measured by DLS at selected time points within 18 h at 37 °C. The samples contain 10 μ g pDNA-GFP.

was also counterchecked by simple observation (organoleptic) (no visible aggregation and sediment, data not shown).

2.2. Hemolysis Assay

For the intravenous application of nanoparticles, the in vitro analysis of the interactions with erythrocytes is relevant for biocompatibility. Especially positively charged particles can interact with the negatively charged erythrocyte membrane.^[30] This can result in lysis of the erythrocytes and release of hemoglobin, lactate dehydrogenases, and potassium with the risk for hemolytic anemia, icterus, hemoglobinuria, severe kidney damage, and thrombosis.^[31]

The lipoplex formulation was incubated with human erythrocytes and the free hemoglobin concentration was measured spectrophotometrically at 540 nm to screen for hemolytic events. This method complies with the ASTM International Designation F756-17D guidelines. Six increasing lipid concentrations of the OH4:DOPE pDNA-GFP lipoplexes from 1.25 to 200 μ g mL⁻¹ were analyzed. The lipoplex formulation was non-hemolytic in a wide concentration range (up to 125 μ g mL⁻¹, Figure 3), despite of its highly cationic zeta potential (61.7 mV, see Table 1).

2.3. In Vitro Cell Studies

In vitro testing of OH4:DOPE lipoplexes was performed with cell lines representing the first-contact cells after systemic administration, namely, blood vessel endothelial cells and monocytes/macrophages. Human umbilical vein endothelial cells (HUVEC) and human monocytic cells derived from an acute monocytic leukemia patient (THP-1) were chosen for this pre-test. The THP-1 cells were used with and without stimulation with phorbol-12-myristate-13-acetate (PMA) for differentiation into a macrophage-like phenotype. According to

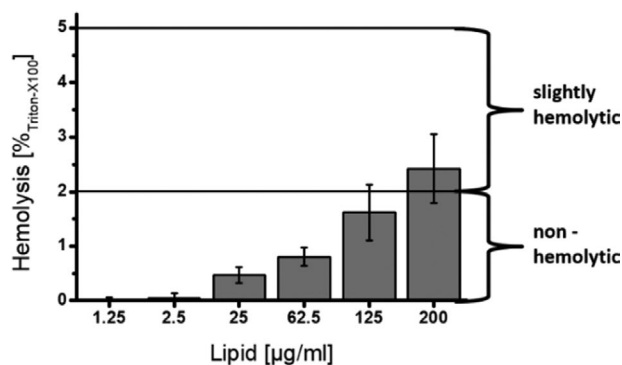


Figure 3. Results of the hemolysis assay of OH4:DOPE pDNA-GFP lipoplexes with increasing concentrations (1.25–200 μ g mL⁻¹ lipid concentration). The hemolytic activity was classified according to the ASTM International Designation F756-17 ($n = 3$).

our previous studies with this formulation,^[23–26] we focus on 24 h experiments and 1.6 μ g DNA per well, keeping in mind that future clinical applications will accompany with extensive dose titration experiments. The transfection efficiency of the OH4:DOPE lipoplexes, either loaded with pDNA-GFP or with mRNA-GFP, was pre-screened by the GFP assay, a reporter gene assay allowing fast quantification by determining the fluorescence of cells. The results were compared with the commercially available Lipofectamine 2000 as gold standard for lipofection. Additionally, the effect of the fluorescent label Rho-DOPE in a molar ratio of 0.5% in the lipid mixture on the transfection efficiency in HUVEC was investigated.

The screening of the transfection efficiency of the different lipoplex formulations in HUVEC cells showed very high mRNA transfection efficacy for the OH4:DOPE formulation and for Lipofectamine 2000 (Figure 4A). Lipofectamine 2000 mRNA-GFP lipoplexes could achieve the highest fraction of GFP expressing cells with \approx 63% after 24 h of incubation. In comparison the OH4:DOPE mRNA-GFP lipoplexes achieved \approx 45% for the unlabeled and \approx 53% GFP positive cells for the Rho-DOPE labeled lipoplexes, a significant lower efficacy. The fluorescence label had no significant effect on the mRNA transfection efficiency in HUVEC cells. Also, the comparison of labeled and unlabeled OH4:DOPE pDNA-GFP lipoplexes showed no significant difference in the transfection rate (labeled \approx 10% and unlabeled \approx 17% GFP positive cells, Figure 4A). Lipofectamine 2000 pDNA-GFP lipoplexes (35%) were more efficient, but not significantly. The uncomplexed nucleic acids could not transfect any cell and did not lead to measurable GFP expression.

Transfection analysis in human monocytes and macrophages showed relatively low efficacy values (Figure 4B). In the case of the transfer of mRNA-GFP into THP-1 monocytes, OH4:DOPE lipoplexes achieved the best results with 3.3% GFP-positive cells. After stimulation with PMA, the monocytes are transformed into M0 macrophages with phagocytotic properties. For the transfection of M0 macrophages the efficacy of the OH4:DOPE mRNA-GFP formulation was 1.7%. Lipofectamine 2000 mRNA-GFP lipoplexes achieved slightly higher values, but not significant.

To summarize, in vivo experiments in 2D cell cultures demonstrated that OH4:DOPE is a highly efficient transfection

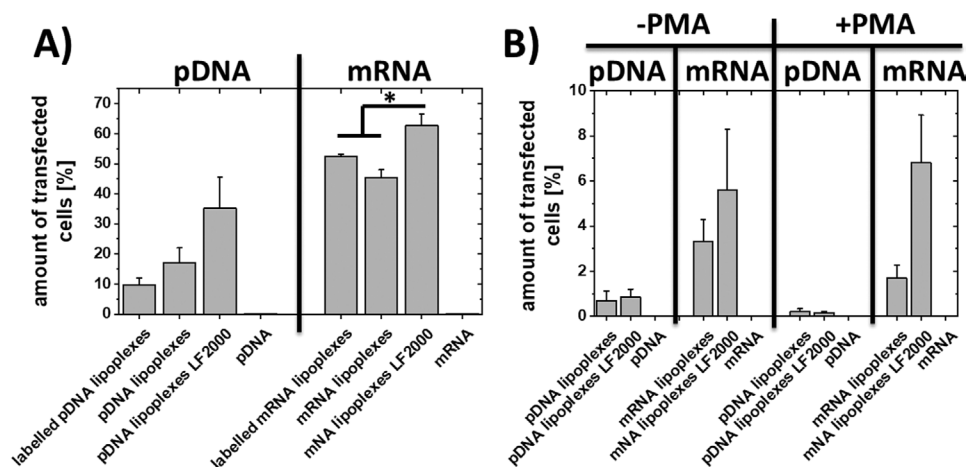


Figure 4. FACS analysis after incubation of different cell types for 24 h with OH4:DOPE lipoplexes loaded with pDNA-GFP or mRNA-GFP: A) HUVEC (human umbilical vein endothelial cells), B) THP-1 (human acute monocytic leukemia cells) cells before and after stimulation with PMA. Transfection efficiency was determined by gating cells on FSC-A versus FITC-A (GFP) as % GFP-positive cells. The cells were treated in a 6-well-plate with different lipoplex solutions containing 1.6 μg nucleic acid per well. The investigations were performed with flow cytometry. The results are from triplicates and statistical analysis was performed using the Mann–Whitney–Wilcoxon-test with an α of 0.05; * $p < 0.05$; $n = 3$). Representative dot-plots of the results presented in (A) are given in Figure S3, Supporting Information.

reagent for endothelial cells. The macrophage cell lines could be transfected to a certain extend with mRNA loaded lipoplexes, while pDNA transfection was barely detectable. The in vitro efficacy of Lipofectamine 2000 was not reached. We would like to note that a screening strategy based only on cell culture models would result in an abandoning of the OH4:DOPE formulation because no benefit compared to Lipofectamine 2000 was proven. In the ongoing part of the manuscript we prove misleading information of the in vitro results and present alternative complex screening models under in vivo conditions. The advantages of alternative screening models, namely CAM and zebrafish embryo, is the cost efficiency compared to mammalian models and the classification as models according to the 3R guidelines.

2.4. HET-CAM Experiments

First in vivo studies on transfection efficiency were performed with the chicken chorionallantoic membrane (CAM). The CAM model is a borderline case between in vitro and in vivo systems and allows the screening of transfection efficiency in a complex tissue consisting of primary cells. No approval as animal experiment is necessary if the experiments comply with the time frames given by national legislation. The choice of the CAM in the here presented test strategy is based on our former experience^[14,16–18] and experiments published from other groups.^[15,32] Due to the high costs of mRNA-GFP we focused on pDNA-GFP for this first approach. The transfection study was performed by the injection of 100 μL OH4:DOPE pDNA-GFP lipoplexes (1 mg mL^{-1} ; containing 0.5 μg pDNA-GFP) into the mesoderm of the CAM on EDD (embryo development day) 10 (see Figure 5A). The injection side of the CAM was dissected after 24 h incubation to take micrographs. Lipofectamine 2000 was used as reference formulation. As negative control, 100 μL 0.9% NaCl solution was injected into the mesoderm. Transfection

efficiency was evaluated by counting the GFP-positive cells (Figure 5B–D). OH4:DOPE pDNA-GFP lipoplexes reached a value of ≈ 200 GFP-positive cells per mm^2 . Lipofectamine 2000 pDNA-GFP lipoplexes, resulted in the low value of 3 GFP-positive cells per mm^2 , in concordance to previous studies.^[14] Thus, the complex tissue of the CAM was better accessible for transfection with OH4:DOPE than with Lipofectamine 2000, which is in contrast to the observation made in the in vitro testing presented above, confirming the lack of predictability of in vitro experiments in the present case. The transfected cell type was not determined in detail, nevertheless the cellular shape indicates probable transfection of fibroblasts.^[14,16]

In addition to the transfection efficacy tests, the chicken embryo was also used to screen acute toxic events. For this purpose the formulation has to be injected intravenously via CAM blood vessels to allow the systemic circulation of the nanomedicine. In our experimental setup the lipoplex formulation was administered in 6 fertilized hens egg embryos on EDD 12 (100 μL of OH4:DOPE lipoplexes with the lipid concentration of 2.5, 25 and 50 $\mu\text{g mL}^{-1}$ as duplicates). After incubating three of the treated eggs (one of each concentration) for 24 h and the other three eggs for 48 h, no toxic effects were visible (screened for heartbeat of the embryo and bleeding events at the CAM membrane), comparable with the negative control (physiological NaCl solution). In conclusion, OH4:DOPE lipoplexes showed no detectable acute toxic effects in the applied model.

2.5. In Vivo Studies Using the Zebrafish Embryo Model

As mentioned previously, the zebrafish embryo represents an efficient model to screen nanomedicines in vivo.^[19] Comparable to CAM experiments no permission for animal experiments is needed if the time frames were considered given by national regulations, consequently, zebrafish larvae are an attractive model according to the 3R strategy. The experimental

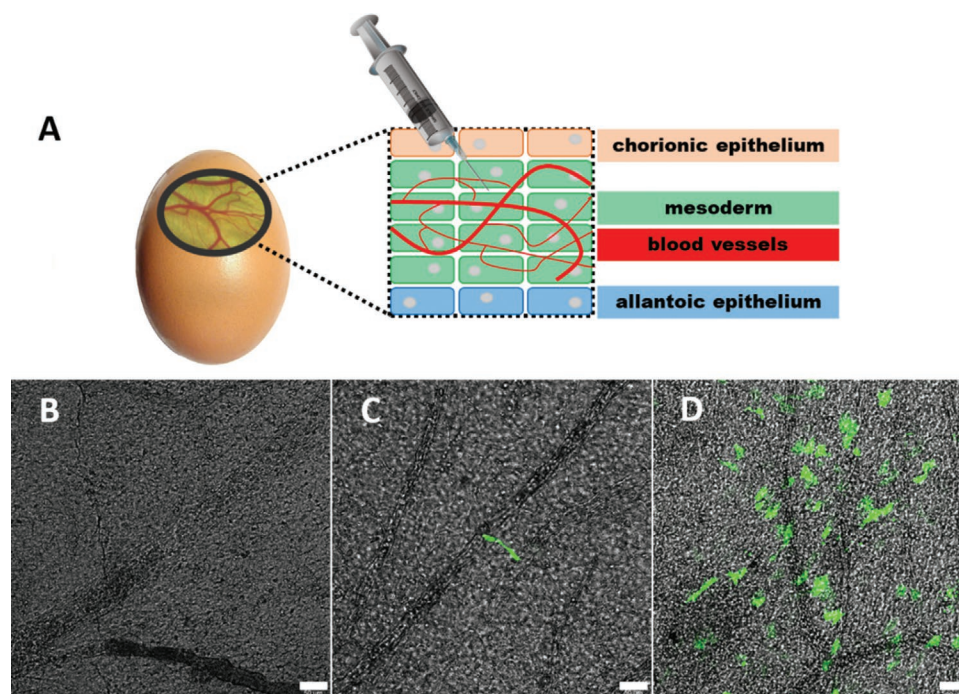


Figure 5. A) Schematic illustration of the CAM transfection experiments. CLSM images showing GFP expression (green) in the mesoderm 24 h after injecting: B) 0.9% sodium chloride, C) Lipofectamine 2000 lipoplexes containing 0.5 µg pDNA-GFP, D) OH4:DOPE lipoplexes containing 0.5 µg pDNA-GFP. Scale bar: 50 µm. The images are representatives of triplicates.

conditions allow evaluating the distribution of fluorescence-tagged nanoparticles using (confocal) fluorescence microscopy for several individuals simultaneously. To investigate biodistribution of OH4:DOPE lipoplexes in the vascular system after intravenous administration the formulations were injected in six zebrafish embryos (age of 52–56 h) intravenously into the Duct of Cuvier (**Figure 6A**). At this developmental stage most of the organ systems are established and the heart starts beating.^[33] OH4:DOPE lipoplexes containing 0.3 ng pDNA or mRNA and labeled with 0.5 mol% Rho-DOPE were used for the in vivo particle tracing in living fish embryos by confocal fluorescence microscopy. The strength of this study was further improved by the use of the *kdrl*:GFP-line, which permanently expresses GFP in blood vessel endothelial cells. No acute toxic effects on the zebrafish embryos (death of the embryo) were observed and it was possible to screen the same animal at different time points to obtain pharmacokinetic information. The embryos were analyzed 14, 24, and 48 h post-injection (hpi). The images demonstrate the circulation of the lipoplexes and their distribution in the vascular system throughout the embryo; while mRNA lipoplexes and pDNA lipoplexes showed a comparable nanoparticle distribution (see **Figure 6**, including schematic illustrations in A and B for orientation).

The details in **Figure 6E** show that lipoplexes were observed in arteries and venous vessels, with the highest quantities in the caudal vein and the CHT-EC. Also, an association of the particles with endothelial cells of arterial and venous vessel walls was detectable (location of the Rho-DOPE signal close to the GFP expressing endothelial cells, see for example at the caudal vein in **Figure 6F/G**), an observation which was described also in previous studies on a cationic liposomal formulation

1 hpi.^[20] However, contrary to this the distribution pattern of the OH4:DOPE lipoplexes does not change significantly within 48 hpi (see **Figures S4, S5**, Supporting Information). Thus, an affinity of the lipoplex formulation to blood vessel endothelial cells could be demonstrated which was not connected with severe aggregation effects resulting in embolic events. Such close contact between cells and lipoplexes is also needed for efficient transfection events, as is explored further in the present study.

The pharmacokinetic investigation in *kdrl*:GFP-zebrafish embryos showed large Rho-DOPE-positive structures in the CHT-EC tissue in the screened time frame which are not colocalized with endothelial cells (see **Figure 6E**, blue triangles). Experiments with *mpeg*:GFP transgenic zebrafish embryos, which bear GFP expressing macrophages, indicate that OH4:DOPE lipoplexes loaded with either DNA or mRNA are also colocalized with macrophages in the CHT-EC tissue (**Figure 7A**, white arrows, green = GFP⁺ macrophages, magenta = Rho-DOPE labelled lipoplexes). This observation indicates phagocytosis of the lipoplexes.

To evaluate the in vivo transfection efficiency of the OH4:DOPE lipoplexes, wild type zebrafish embryos (AB/TL, no cells with specific fluorescence labelling) were injected intravenously into the Duct of Cuvier 52–56 hpf (12 individuals per formulation) using GFP encoding pDNA or mRNA as reporter gene. Comparative analyses of mRNA and pDNA loaded lipoplexes of the formulation OH4:DOPE with Lipofectamine 2000 were performed. Transfection efficiency was evaluated by confocal fluorescence microscopy 12, 24, and 48 hpi, counting the GFP-positive cells per fish (see **Figure 8**). As negative control PBS was injected intravenously. In

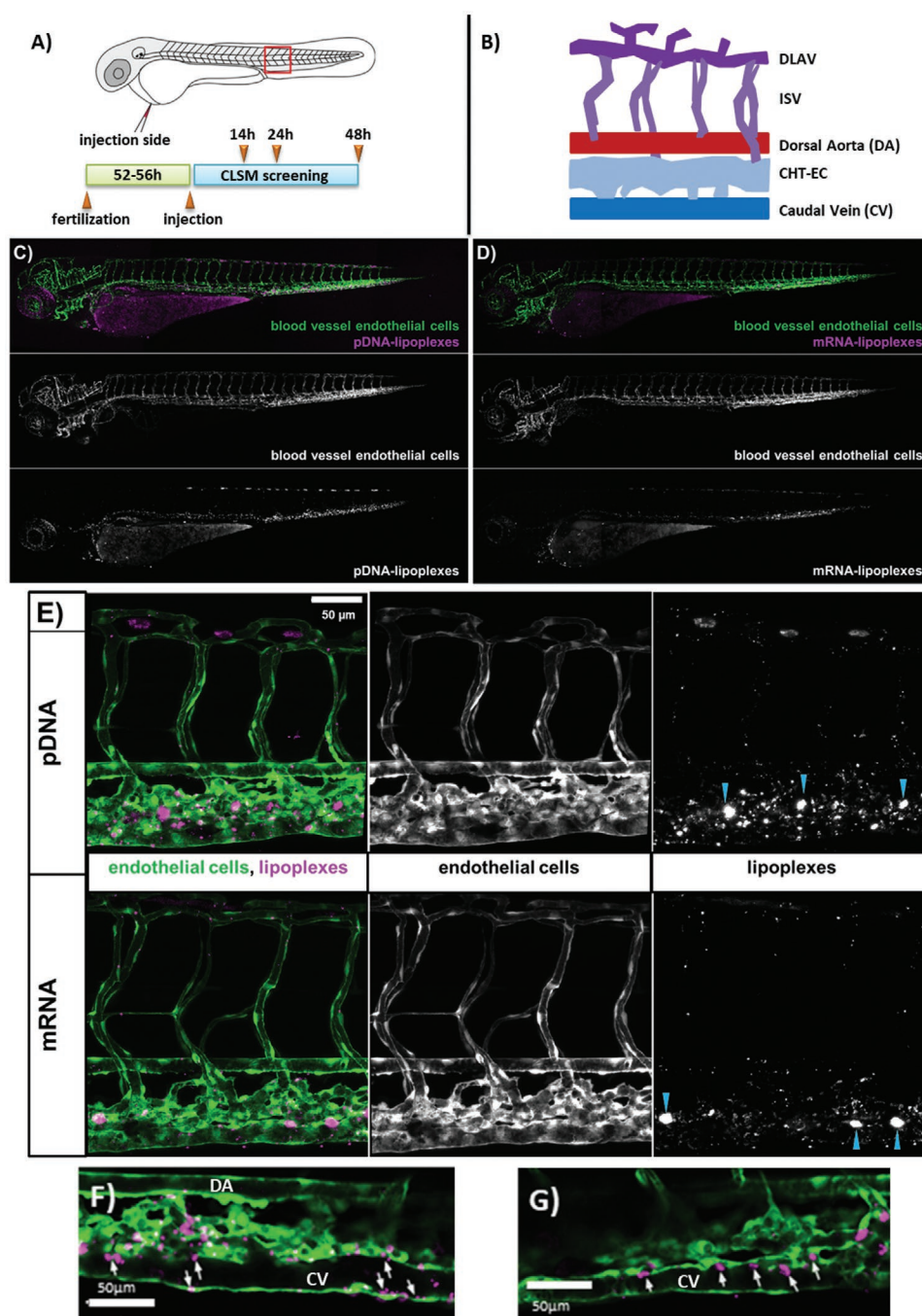


Figure 6. A) Schematic habitus of the zebrafish embryo 54 hpf with highlighted injection side (Duct of Cuvier, a big vein) and indicated region for detailed analysis of vascular distribution (red square). Furthermore a time line for the experimental setup is given. B) The highlighted region (red square in A) as blood vessel map: CHT-EC = caudal hematopoietic tissue endothelial cells; DLAV = dorsal longitudinal anastomotic vessel; ISV = intersegmental vessel. C–G) Representative micrographs of biodistribution studies of OH4:DOPE lipoplexes after intravenous administration into transgenic fish lines *kdrl:GFP* 52–56 hpf. In the multiple color images GFP fluorescence is shown in green (permanently expressed in blood vessel endothelial cells of the *kdrl:GFP*-line) and the Rho-DOPE label of lipoplexes in magenta. Additionally, both channels are shown in separate images in grey scale. The shown individuals are representatives of a series of experiments with 6 embryos per lipoplex formulation (overview: Figures S4 and S5, Supporting Information). Overview images of the entire embryo 24 hpi are shown in C) for pDNA loaded lipoplexes and D) for mRNA loaded lipoplexes. E) Detailed images of the region caudal to the cloaca 24 hpi for pDNA (upper panels) and mRNA (lower panels) loaded OH4:DOPE lipoplexes as merged image as well as single channels. Example of single optical slices through the caudal vein (CV) 14 hpi with lipoplexes attached to the vessel wall (indicated by white arrows) for F) pDNA- and G) mRNA-loaded lipoplexes.

addition, “uncomplexed” mRNA and pDNA was administered to zebrafish embryos to analyze the transfection enhancing effect of the lipid vectors.

First, lipoplex injections were performed using Rho-DOPE-labeled lipoplexes to document successful injection and distribution of lipoplexes in the embryo for the transfection

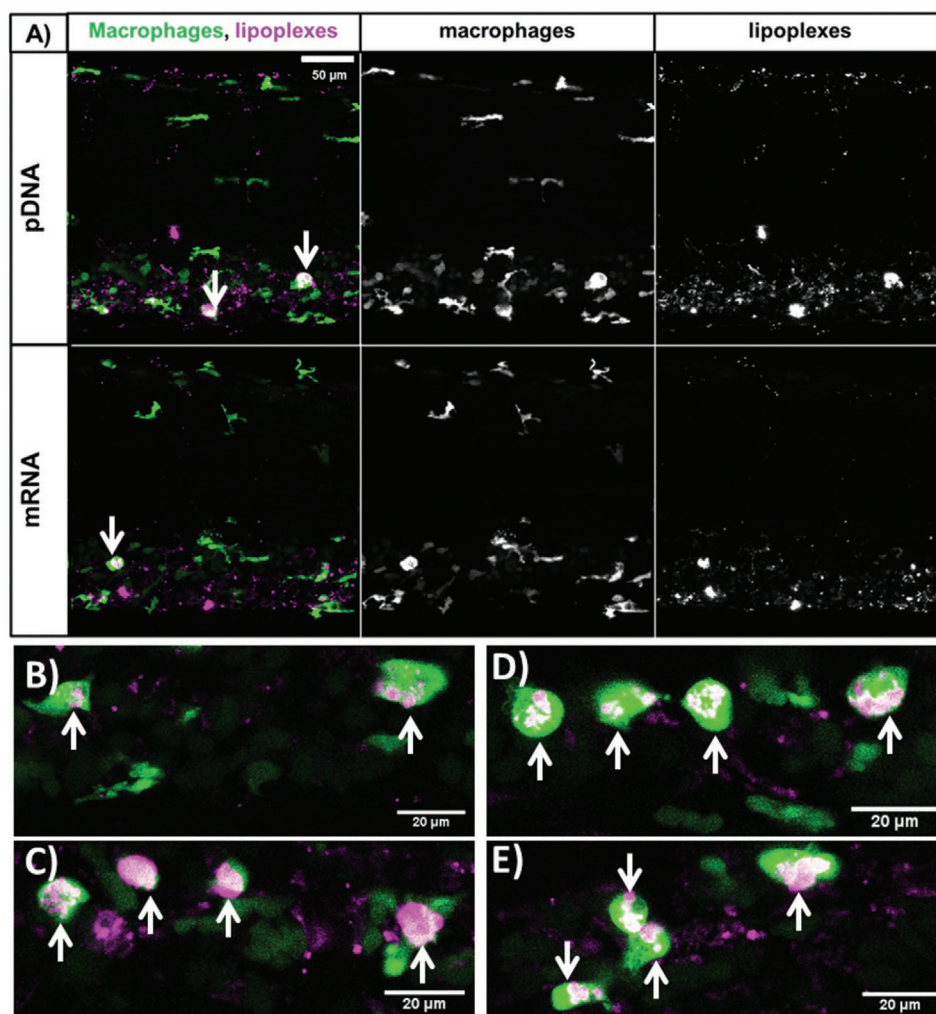


Figure 7. A) Biodistribution studies of OH4:DOPE lipoplexes using the *mpeg*:GFP fish line which is characterized by GFP expressing macrophages after intravenous administration. In the multiple color images GFP is shown in green (permanently expressed in macrophages of the *mpeg*-line) and the Rho-DOPE label of lipoplexes in magenta. Additionally, both channels are shown in separate images in grey scale. The shown micrographs of the region caudal to the cloaca 24 hpi are representatives of a series of experiments with 6 embryos per lipoplex formulation (overview: Figures S6 and S7, Supporting Information). B–E) Details (single optical slice) of macrophages (green, *mpeg*:GFP fish line) within the CHT-EC tissue 14 hpi of B/C) pDNA- and D/E) mRNA-loaded OH4:DOPE lipoplexes at N/P 4 labelled with Rho-DOPE (magenta) colocalized with macrophages (green). Colocalization events are indicated by white arrows.

experiments. The experiments show the expected distribution of the lipoplexes according to the pharmacokinetic experiments described above, and an efficient nucleic acid transfer was detected resulting in GFP-positive cells (Figure 8). For further investigations, un-tagged lipoplexes were injected and GFP-positive cells counted (examples Figure 8A/B). Unexpectedly, these un-tagged lipoplexes were significantly more efficient compared to the Rho-DOPE labelled lipoplexes (contrary to the in vitro experiments presented above showing no significant difference). This can be partly explained by the physicochemical characterization data of the labeled and unlabeled lipoplexes loaded with pDNA-GFP or mRNA-GFP, which showed that the labelled ones have a lower zeta potential (see Table 1). The difference in the zeta potential of the lipoplexes could affect the composition of the protein corona, and consequently, might change the transfection efficiency.^[34]

When comparing Lipofectamine 2000 with the OH4:DOPE formulations, a significant higher efficacy of OH4:DOPE was observed (Figure 8). For mRNA-GFP lipoplexes Lipofectamine 2000 showed significant higher transfection rates than the Rho-DOPE labelled OH4:DOPE formulation, but the unlabeled OH4:DOPE formulation was significantly the most efficient formulation (Figure 8D). Lipofectamine 2000 pDNA-GFP lipoplexes achieved significant lower transfection rates than OH4:DOPE pDNA-GFP lipoplexes (see Figure 8C). The differences in efficacies of pDNA and mRNA loaded lipoplexes of the same type of transfection reagent can be explained by the action side of the nucleic acid. While mRNA delivery systems solely have to overcome the cell membrane/endosomal membrane, a pDNA delivery system additionally has to overcome the nucleus membrane for efficient transcription.

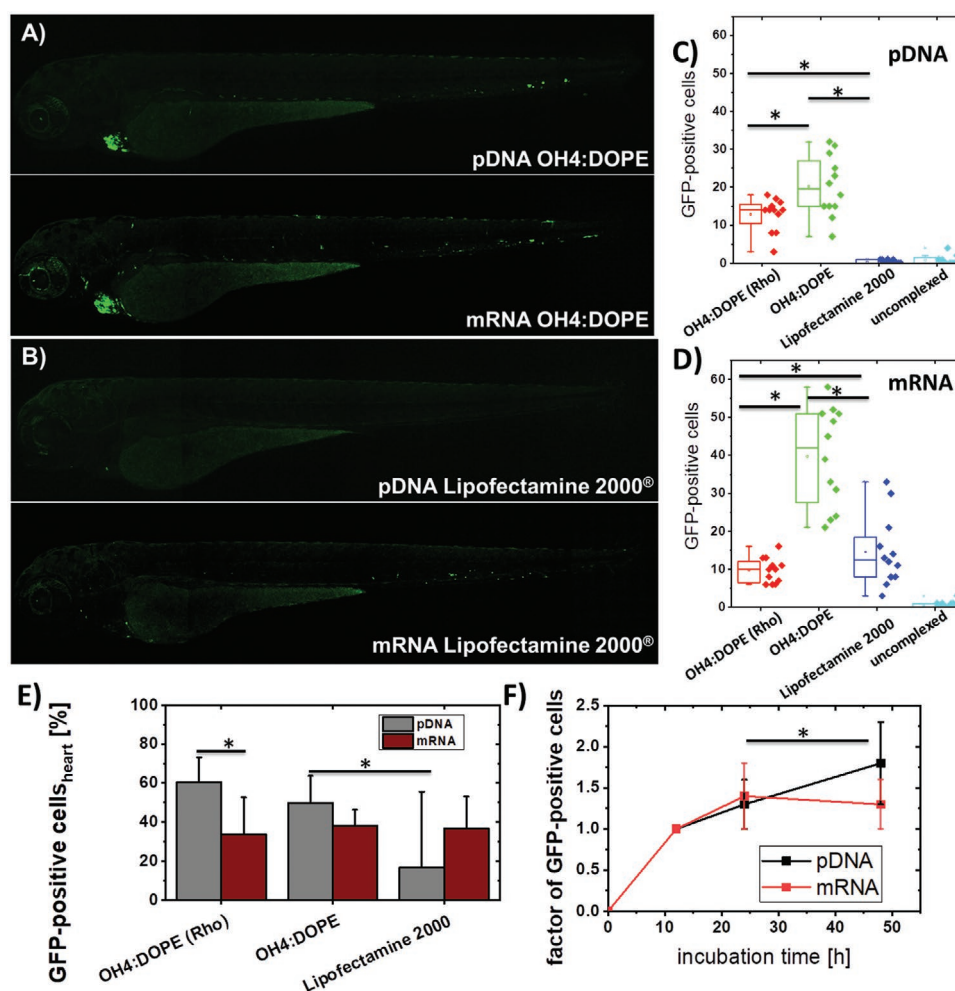


Figure 8. A,B) CLSM image of the GFP expression in living zebrafish embryos after injection of 2 nL lipoplex formulation containing 0.3 ng nucleic acid 24 hpi. The lipoplexes were injected into the Duct of Curvier in AB/TL fish embryos. The GFP signal, which results from the reporter gene of the administered mRNA-GFP or pDNA-GFP, is presented in green. Following representative comparisons are shown A) pDNA-GFP and mRNA-GFP loaded OH4:DOPE lipoplexes, B) pDNA-GFP and mRNA-GFP loaded Lipofectamine 2000. Boxplot of the GFP positive cells in AB/TL zebrafish embryos 24 hpi of C) pDNA- or D) mRNA-loaded lipoplex formulations. All individuals are shown in the Figures S8–S15, Supporting Information. E) Relative amount of GFP-positive cells in the region of the heart 24 hpi compared to the total number of GFP-positive cells in each fish. F) Pharmacodynamic evaluation of the GFP expression over an incubation period of 48 h after injection of OH4:DOPE lipoplexes loaded with pDNA or mRNA. The labelling of significance belongs to the pDNA curve. Significant differences determined by one-way-ANOVA test with post Turkey test ($n = 12$, $\alpha = 0.05$, $p < 0.05$) are labelled with stars.

The time dependent evaluation of GFP expression demonstrate that the number of GFP-expressing cells after transfection with pDNA-loaded lipoplexes increases during the 48 h screening after injection. In contrast, after application of mRNA-loaded lipoplexes the transfection maximum was reached after 24 h (see Figure 8F). This result is comparable with previous *in vitro* and *in vivo* studies with other non-viral transfer vectors.^[35]

When we evaluated the number of GFP positive cells we noticed that the OH4:DOPE lipoplexes (pDNA-GFP or mRNA-GFP) treated fish showed a special transfection pattern with an increased occurrence of GFP-positive cells in the region of the heart (see Figure 8A). Quantitatively, 50% of the GFP-positive cells transfected by the pDNA lipoplex formulation and 38% of the GFP-positive cells transfected by mRNA lipoplexes were located at the heart (see Figure 8E). Comparing the small area

of the endocardium with the area of all blood vessels these numbers demonstrate a high preference for the heart.

Thus, the zebrafish embryo studies described above raise two questions: i) Which cell type is transfected? and ii) Why a preferred transfection at the heart was seen? Shape and localization of most of the transfected cells suggest that the endothelial cells were preferably transfected. Furthermore, the evidence of phagocytic uptake in the biodistribution studies illuminates the possibility that macrophages got transfected. Two transgenic fish lines were chosen to experimentally prove these suggestions: The *kdr1*:RFP line which expresses RFP in blood vessel endothelial cells and a transgenic fish line with RFP expressing macrophages (*mpeg*:RFP). The transgenic embryos were injected in the same manner as the AB/TL zebrafish embryos for the transfection experiments. The analysis of the transfected cell type was performed by screening for co-localization of the

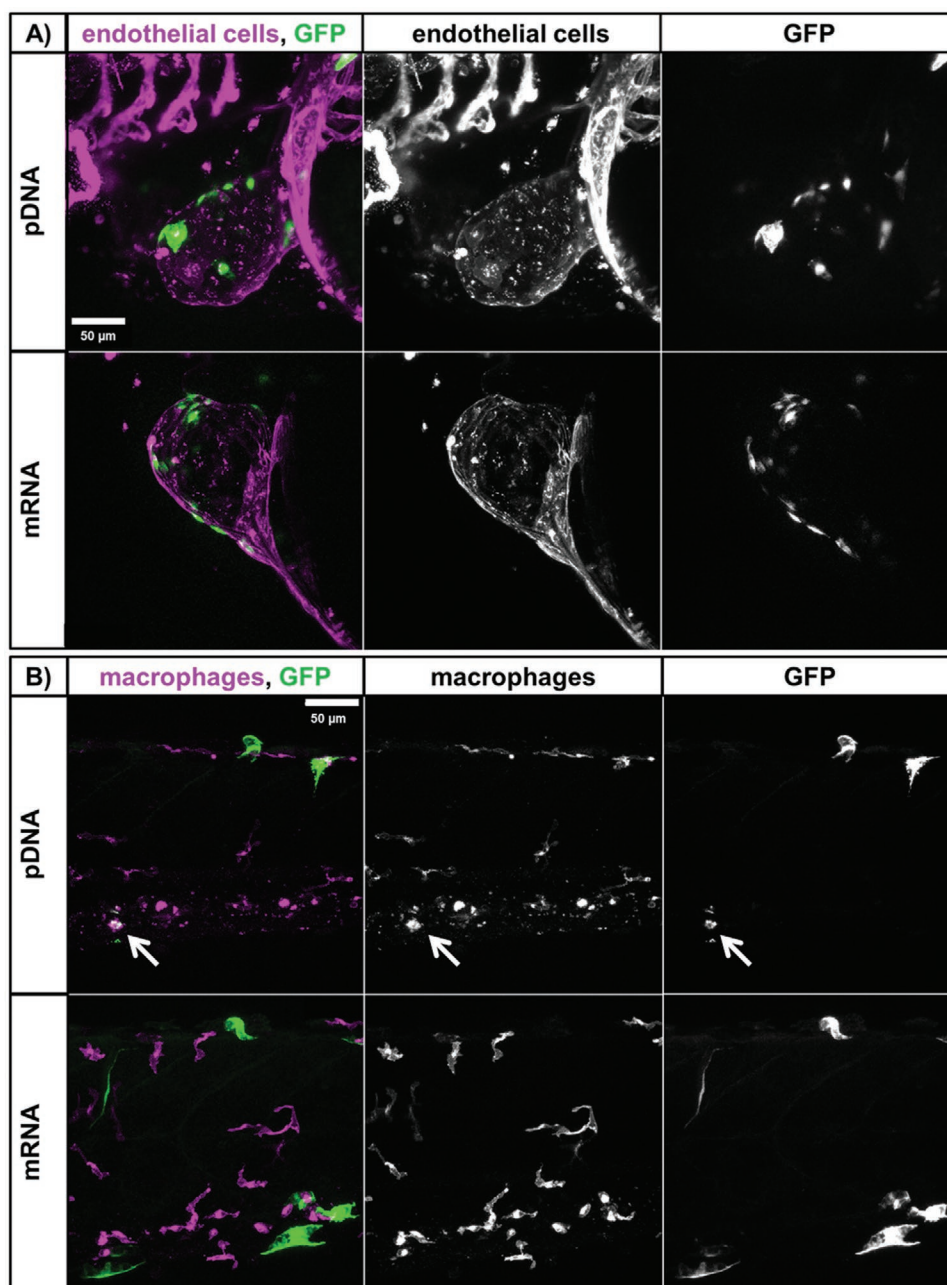


Figure 9. Detailed confocal fluorescence micrographs of transgenic fish lines: A) heart region of *kdrl*:RFP embryos (representative of 6 individuals which are presented in Figures S16 and S17, Supporting Information) and B) the region caudal to the cloaca of *mpeg*:RFP 24 h after injection of OH4:DOPE N/P 4 lipoplexes loaded with pDNA-GFP or mRNA-GFP (nucleic acid dose was 0.3 ng). The lipoplexes were injected intravenously in the Duct of Cuvier of 52–56 h old zebrafish embryos. In the multiple color image GFP (reporter gene) is shown in green and the RFP (transgenic endothelial cells or macrophages) in magenta. Single channel images are shown in the middle and on the left side. Colocalization of GFP and RFP in macrophages is indicated by the white arrow.

GFP fluorescence (successful transfection with the reporter gene) and the RFP fluorescence (transgenic label of endothelial cells or macrophages) by confocal fluorescence microscopy.

First, we will focus on the macrophages. These studies demonstrated that only lipoplexes containing pDNA-GFP can transfect macrophages (see Figure 9B, GFP and RFP co-localization, and Figure S18, Supporting Information). The GFP-positive and RFP-negative cells which were additionally observed are

probably endothelial cells according to their shape. Nevertheless, it has to be considered, that GFP-containing cell debris of other transfected cells phagocytosed by macrophages also results in such co-localization events. High shape conformity between GFP and RFP signal is a strong hint for a macrophage transfection. Contrary to the in vitro cell culture experiments with THP-1 cells, we could not detect mRNA-GFP transfected macrophages in the zebrafish embryo (compared Figure 9B

with Figure 3B), although mRNA lipoplexes were found in macrophages (Figure 7). Obviously, the escape out of the phagolysosome is not given.

The second focus was the transfected cell type at the heart. The detailed images of different zebrafish hearts showed a large number of GFP-positive endocardial cells with a high fluorescence intensity in both cases, for transfection with DNA and for transfection with mRNA. The RFP-labeled endothelial cells clearly showed the co-localization with GFP and the congruency of both signals allows the assumption that the green fluorescent cells are endothelial cells (see Figure 9A; Figures S16, S17, Supporting Information). To rule out the possibility that the transfection of the endocardial cells is an effect caused by the injection site, additional embryos were injected intravenously into the tail above the yolk. The change of the injection site also leads to a transfection of endocardial cells (see Figure S19, Supporting Information).

Concluding, OH4:DOPE pDNA-GFP and mRNA-GFP lipoplexes, can reproducibly transfect endothelial cells with preference for the heart, independent of the injection site. But why does the injection of positively charged lipoplexes lead to the selective transfection?

There is no evidence from databases that endothelial cells of the heart have a special receptor/transporter pattern compared to vascular endothelial cells. Hence physical mechanisms can answer this question. The zebrafish heart is similar to the human heart in physiology and structure. The main difference to the biventricular mammalian heart is that the adult zebrafish heart is composed of one ventricle, one atrium, one atrioventricular valve, and one outflow valve. The development of the heart starts with the specification of precardiac cells 5 hpf. Following its formation, the heart has the shape of a disk, elongates and looped into a linear heart tube. This linear heart tube is composed of two cell layers separated by an acellular gelatinous extracellular matrix layer (cardiac jelly). The inner layer is composed of endocardial cells and the outer layer is composed of contractile myocytes. The first rhythmic heart beat starts 24 hpf. After 48 hpf the major components of the heart were formed. At this developmental stage the heart is located in the pericardial cavity and two chambers have been developed and the ventricular chamber balloons out. At this stage, cardiomyocytes start trabeculation from the ventricle wall and 72 hpf the ventricle of the embryo has obvious trabecular ridges to increase myocardial surface for blood oxygenation.^[33,36,37] This trabeculation in the ventricle could be a reason for the increased transfection events in the heart. The surface area is increased and rougher compared to other blood vessels, allowing a more efficient adsorption of positively charged lipoplexes. Furthermore, cell division is increasing in this area because the heart is still in development. During cell division, the DNA transfer into the nucleus is more efficient using non-viral nucleic acid vehicles, what may explain a higher efficacy of pDNA lipoplex transfection.^[38] Nevertheless, this would not explain the efficient heart transfection with mRNA loaded lipoplexes. Also turbulence patterns in the blood flow in the heart of the developing embryo can be a hypothesis for the preferred endocardial transfection. Due to the balloon-like protrusion of the atrium and ventricle, a vortex is formed in the atrium resulting in particle retention.^[36] Also, in the trabecular ridges turbulent flow patterns occur,

were a retention of particles could be favored.^[39] Nevertheless, further experiments are necessary to determine the exact reasons of this phenomenon.

2.6. In Vivo Gene Delivery in Mice After Systemic Administration

As the mouse is the most broadly used mammalian laboratory animal and testing procedures are well defined, we evaluated in a pilot study the transfection properties of OH4:DOPE lipoplexes after systemic administration focusing on the more difficult pDNA transfection. Lipoplexes at N/P 4 based on firefly luciferase plasmid were injected via the lateral tail vein and transfection tracked via bioluminescence imaging. The plasmid employed for these studies, pCpG-hCMV-EF1a-LucSH, is based on a CpG free backbone which enables high and sustained transgene expression.^[40,41] Lipoplexes were prepared in 5% glucose (final concentration) to have them in a physiological medium and investigated for size distribution as a quality-control check prior to intravenous injections. The hydrodynamic diameter of OH4:DOPE lipoplexes under this conditions was at 150 nm (mode of the distribution, Figure S20, Supporting Information) and similar to the other results from DLS based size distribution. Mice were imaged 24 and 48 h after administration of lipoplexes. As shown in Figure 10, a clear bioluminescence signal was observed at both time points in the thoracic area indicating luciferase gene expression and thereby successful gene delivery in vivo. The bioluminescence signal seems to be in both the lungs indicating efficient lung-transfection, which was validated by ex vivo organ imaging. Bioluminescence signal can be clearly observed only in the lungs, as shown in Figure S21, Supporting Information. The remaining organs of treated mice do not show any signal, as also visible in comparison to organs from control mouse. This observation confirms successful DNA delivery to lungs in vivo via OH4:DOPE lipoplexes, after they were administered systemically and highlights the in vivo transfection potential of these lipoplexes.

It is known, that nanoparticles based on cationic lipids, polycations, or cationic dendrimers with a net positive surface charge interact with plasma proteins or erythrocytes, which leads to their entrapment in the first vascular bed encountered after i.v. injection, namely the lung.^[40,42] Here, we observed a similar effect, that is, direct transfection of lung tissue, while no signal is observed in all other organs.

Of note, the same interaction of cationic nanoparticles with blood components can result in severe side effects. Above, we have shown that the lipoplexes do not cause hemolysis in a wide concentration range, and acute toxicity was not observed in the chicken embryo as well as the zebrafish embryo. The herein presented pilot study in mice also shows that the lipoplexes were well tolerated, without any acute respiratory distress. Both, cationic lipids and polycations can induce mild to severe liver damage, mainly microvesicular fatty liver.^[43] The histopathological analysis of examined organs from OH4:DOPE NP4 pDNA lipoplex treated and control animals demonstrated healthy and physiological cell and tissue structures (Figure S22, Supporting Information). In the liver there were no obvious alterations, as

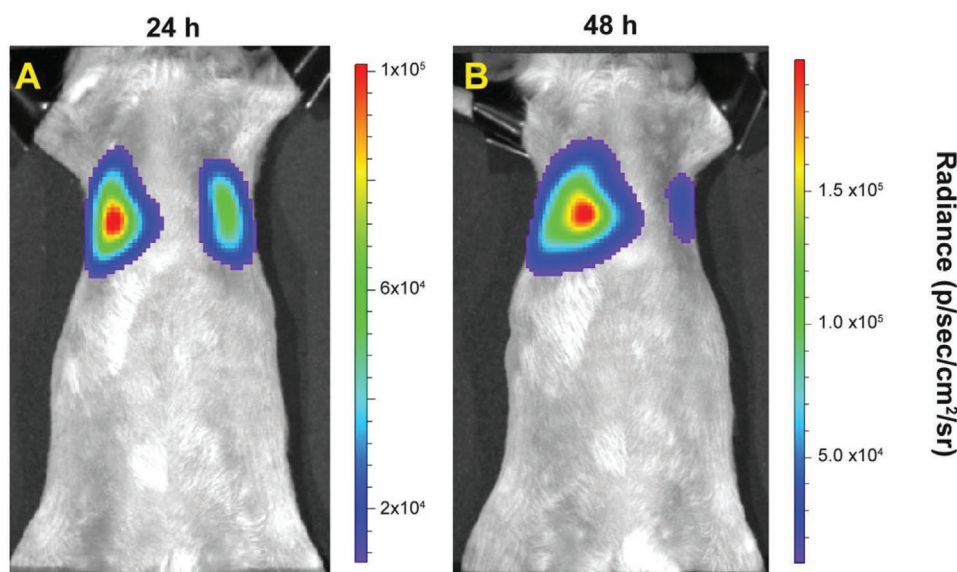


Figure 10. Bioluminescence imaging (BLI) based investigation of in vivo transfection by DNA lipoplexes in mice. Firefly luciferase reporter gene based N/P4 lipoplexes were intravenously injected at a dose of 2.5 mg kg^{-1} and transfection status followed at a) 24 and b) 48 h after administration via BLI of animals. The images show BLI signal (in radiance; color coded as per the scale shown on the right) overlaid on reflected light images from a representative animal.

no fatty liver degeneration or alteration of hepatocytes was visible. As well as no signs of steatosis or fibrosis was observed, although some age related structural changes could be seen. All mice exhibited functional portal hepatic veins with homogeneous smooth liver parenchyma. Within lung parenchyma of treated animals, terminal bronchioles and alveolar ducts were visible with no lesions. Neither inflammatory processes nor oedema was observed compared to the control group. Also there were no signs of structural damages to pneumocytes and lung parenchyma.

Taken together, OH4:DOPE based lipoplexes in conjunction with a CpG-free plasmid allows efficient transgene expression in lung whilst avoiding gross liver toxicity.

3. Discussion of the Different In Vivo Models Used in this Study

The CAM of the chicken embryo is a very simple model system allowing in vivo tests according to the 3R guidelines. The power of the CAM model is the small scale maintenance compared to mammalian models and the possibility to make experiments with living vertebrates without the need of animal experiment permission if the restricting time frames are fulfilled. The strength of the model used in the herein described way is the possibility to check for transfection efficiency in a complex tissue by a non-invasive administration on the ectoderm, or an injection into the more complex mesoderm.^[14] Also the screening of acute toxicity by an administration to the systemic circulation of the embryo is possible. Nevertheless, biodistribution screening in chicken embryos is not established yet. For that purpose we demonstrated the power of the zebrafish embryo model which evolves the full potential in biodistribution screening of fluorescence-tagged formulations

in transgenic fish lines with fluorescent tissues, for example, blood vessels. The main strength of the zebrafish embryo model is the ability to study nucleic acid transfer efficacy in the whole organism. Efficient transfection of reporter gene-encoding mRNA using Lipofectamine 2000 lipoplexes was described after direct injection into the hindbrain ventricle of 48 h post fertilization zebrafish embryos.^[44] Lipid nanoparticles loaded with GFP encoding mRNA were injected in different tissues of the zebrafish larvae and resulted in transfection events.^[22] Both articles show no additional experiments in mammals. Our experiments with reporter gene-encoding DNA and mRNA encapsulated with OH4:DOPE show efficient transfection of blood vessel endothelial cells with a preference for endocardial cells. Consequently, we demonstrated the suitability of the zebrafish embryo model as 3R-based screening strategy for non-viral nucleic acid delivery systems. To our knowledge, this is the first time the transfection efficacy in the zebrafish larvae was compared to experiments in mice. In both species, the absence of severe embolic events could be demonstrated. The experiments in the fish model proved in vivo efficacy of the OH4:DOPE formulation with the preferred transfection of endothelial cells of the endocardium. The pilot studies in mice confirmed the in vivo efficacy of the OH4:DOPE formulation with efficient lung transfection, which is of course absent in zebrafish larvae. Here it would be of interest for follow up studies, how the organ distribution and transfection pattern in zebrafish will change when modifying the lipid composition in comparison to the mouse model, as it has been described recently.^[45] If the organ selective transfection efficiency in the different species is connected to a comparable mechanism is a scientific question which still has to be answered. Comparable physical behavior or forces in the streaming profile of the blood in the fish embryo heart and the mice lung could explain this behavior, but needs experimental approval. Additional studies

Table 2. Comparison of different biological models with respect to their relevance for nucleic acid nanocarrier research (No—not relevant, yes—it is relevant, and yes (partly)—it is partly relevant).

Property of biological model relevant for pre-clinical translation of nucleic acid nanocarriers	In vitro models	In vivo models (rodent/large animal models)	Chick embryo chorioallantoic membrane model (CAM)	Zebra fish larvae model
Physiologically relevant medium/environment (e.g., for stability testing)	No	Yes	Yes (partly)	Yes
Pharmacokinetic and pharmacodynamic aspects (e.g., for bio-distribution screening)	No	Yes	No	Yes
Complex tissue/organ interface (e.g., for transfection efficiency investigation)	No	Yes	Yes (partly)	Yes
Toxicity evaluation (e.g., for nanotoxicity screening)	Yes (partly)	Yes	Yes	Yes (partly)

with other non-viral nucleic acid delivery systems are needed to prove correlations between both models and would pave the way to implement the zebrafish larvae as an accepted model in gene medicine development. We summarized our assessment of the different model systems in **Table 2**.

4. Conclusion

This study combines in vitro screening of hemocompatibility and transfection efficiency with first in vivo evaluations using special animal models according to the 3R rules. The experiments clearly show that in vitro experiments can only reflect a part of reality, because in vitro results can differ significantly from in vivo reality due to the simplified environment which differs from complex tissues. The complexity of tissues can only be represented in a living organism. Therefore, we consider the combination of CAM model experiments and zebrafish embryo model as an efficient screening tool for the examination of nano-scaled non-viral nucleic acid delivery systems prior to rodent experiments. The in vitro experiments performed in this study demonstrated that the investigated lipoplex formulation is stable in the physiological milieu due to its high zeta potential without being hemolytic. However, the formulations of OH4:DOPE pDNA-GFP and mRNA-GFP lipoplexes demonstrated the ability to transfect blood vessel endothelial cells and, to a certain limit, macrophages in vitro, although the efficiency of Lipofectamine 2000 was not reached. But in in vivo experiments the lipoplex formulation OH4:DOPE N/P4 performed much better than the reference. In the CAM, as well as the zebrafish embryo experiments, a higher transfection efficiency for OH4:DOPE lipoplexes was observed compared to Lipofectamine 2000. The efficacy was significantly higher for both, lipoplexes loaded with pDNA and lipoplexes loaded with mRNA in the zebrafish embryo. The demonstrated transfection of endothelial cells (for mRNA and pDNA) in the fish embryo after systemic administration with OH4:DOPE lipoplexes show promising target cells to develop gene therapeutic strategies based on the formulation. Endothelial cells are a promising target for gene therapy to induce the regeneration of blood vessels or reduce the production of adhesion proteins which promote the attachment of leukocytes (transfection with siRNA suppressing the production of adhesion proteins).^[46] Now therapeutic options, especially for blood vessels in the lung, have to be evaluated in more detail in mammalian models. To give

a future perspective, chronic obstructive pulmonary disease (COPD) and pulmonary hypertension are two diseases based on endothelial dysfunction in pulmonary blood vessels.^[47]

In conclusion, the high potential of the multivalent ionizable formulation OH4:DOPE as delivery system for mRNA or DNA which is suitable for in vivo administration was demonstrated. The formulation can also overcome hurdles of complex tissue or blood stream while the protective effect on the nucleic acid cargo was given. Future research will focus on detailed application for specific diseases, while the systemic and local administration strategies can be considered. Furthermore, this article demonstrates the power of the 3R in vivo model systems, namely CAM model and zebrafish embryo, for the preclinical evaluation of non-viral nucleic acid delivery systems.

5. Experimental Section

Materials: All chemicals, unless otherwise specified, were purchased from Sigma-Aldrich/Merck (Steinheim, Germany). 1,2-Dioleoyl-sn-glycero-3-phosphoethanolamine (DOPE) was bought from Avanti Polar Lipids (Alabaster, AL, USA). The pCMV-GFP plasmid, encoding for the green fluorescent protein (GFP), was purchased from PlasmidFactory (Bielefeld, Germany) and has a size of 3487 bp. For the rest of the paper, pDNA-GFP will be used to indicate this plasmid. The CleanCap EGFP mRNA (5moU, 996 b) (Enhanced Green Fluorescent Protein mRNA with 5-methoxyuridine) was bought from TriLink Biotechnologies (San Diego, USA). In the article the term mRNA-GFP will be used. HUVEC cells, cell culture media, the Growth Medium Supplement Mix and phosphate buffered saline (PBS) were bought from Promega (Madison, WI, USA). THP-1 cells were purchased from ATCC (Manassas, Virginia, USA). The synthesis of OH4 (N-{6-amino-1-[N-(9Z)-octadec-9-enylamino]-1-oxohexan-(2S)-2-yl]-N'-2-[N,N-bis(2-aminoethyl)amino]ethyl}-2-hexadecylpropanediamide) was described previously.^[10,23] The fluorescently tagged lipid Rho-DOPE [(1,2-dioleoyl-sn-glycero-3-phosphoethanolamine-N-(lissamine rhodamine B sulfonyl) (ammonium salt), $\lambda_{\text{abs}}^{\text{max}} = 560 \text{ nm}$, $\lambda_{\text{em}}^{\text{max}} = 583 \text{ nm}$] was purchased from Avanti polar lipids.

Liposomes and Lipoplex Preparation: The OH4:DOPE lipid formulation was prepared by the thin-film hydration method by producing a lipid film with the cationic lipid (OH4), the co-lipid DOPE, and the fluorescent labeled Rho-DOPE. Each lipid (OH4, DOPE, and Rho-DOPE) was dissolved separately in a chloroform:methanol (8:2, v:v) to prepare a stock solution with a concentration of 2 mg mL^{-1} . The lipids were combined to a molar OH4:DOPE ratio of 1:1 (n:n) and, if fluorescence labelling was performed, 0.5 mol% Rho-DOPE was added to the lipid mixture. Subsequently, the organic solvent was removed through evaporation for 30 min at 500 mbar followed by 1 h at $\leq 15 \text{ mbar}$. After formation of a dry lipid film, sterile filtrated 10 mM MES buffer solution

(pH 6.5) was added and vortexed to achieve a final lipid concentration of 2 mg mL⁻¹. Afterward, the lipid dispersions were incubated at 50 °C while shaking (1400 rpm) for 30 min (Eppendorf Thermomixer 5436) followed by sonication at 37 kHz for 8 min at 30 °C.

For lipoplex preparation, the OH4:DOPE 1:1 (n:n) (with and without 0.5 mol% Rho-DOPE) liposomes were combined with plasmid DNA (pDNA) or messenger RNA (mRNA) at an N/P ratio of 4 (molar ratio of primary amines in cationic lipids to phosphate groups in nucleic acid). Complexation occurred spontaneously after adding the nucleic acid solution in one step to the lipid formulation followed by gently mixing. The samples were incubated for 15 min at 25 °C until further use.

Dynamic Light Scattering (DLS) Measurements: Correlation functions and the corresponding size distribution curves were measured with a ZetasizerNano ZS ZEN3600 (Malvern Instruments, Worcestershire, UK). The scattering angle was set to 173°. Every measurement consists of three independent measurements of 15 runs with duration of 20 s for each run. The measurements were performed at 25 or 37 °C, as indicated. For the calculations, a viscosity of $\eta = 0.8872$ mPa s and a refractive index of 1.33 for water were assumed. The autocorrelation function was evaluated by the Zetasizer Software 7.3 (Malvern Instruments, Worcestershire, UK) using an exponential regularized fit. For time dependent measurements the laser was set to a fixed position and also attenuation was kept constant.

ζ Potential Measurements: The electrophoretic mobility was measured using laser Doppler electrophoresis technique with a ZetasizerNano ZS ZEN3600 (Malvern Instruments, Worcestershire, UK) and a clear disposable folded capillary cell (DTS1060, Malvern Instruments). Each value was the mean of three independent measurements consisting of 30 runs at a voltage of 60 V. The measurements were performed at 25 °C. For the calculations, a viscosity of $\eta = 0.8872$ mPa s, a dielectric constant of $\epsilon = 78.5$ F m⁻¹, and a refractive index of 1.33 of water were assumed. The mobility μ of the migrating particles was converted into ζ using the Smoluchowski relation $\zeta = (\mu \times \eta) / \epsilon$ (Zetasizer Software 7.3; Malvern Instruments, Worcestershire, UK).

Flow Cytometry: For the transfection measurement HUVEC cells were cultured in Endothelial Cell Growth Medium (Promega, Madison, WI, USA) complemented with the Growth Medium Supplement Mix (Promega, Madison, WI, USA) and THP-1 cells in RPMI1640 medium (Thermo Fisher) supplemented with 10% FCS. Phorbol-12-myristate-13-acetate (PMA) for differentiation into the macrophage-like phenotype was used in a concentration of 150 nM. Cells were cultured at 37 °C, 5% CO₂, and saturated humidity. The cells were cultured as monolayers and were passaged upon reaching 80–90% confluency. For the transfection experiments, passage numbers between 3–8 were used. The cells were seeded in 6-well plates with a density of 1.5×10^5 cells mL⁻¹ and lipoplexes added 24 h thereafter at an amount of 1.6 μ g pDNA or mRNA per well, filled up with PBS to a volume of 700 μ L and incubated for 1 h. Thereafter, 1300 μ L Endothelial Cell Growth Medium was added to each well and incubated for another 23 h at 37 °C. Afterward, GFP-expression was measured by flow cytometry. Trypsinised cells were centrifuged (220 \times g, 5 min, RT) and resuspended in PBS. Per measurement 10 000 cells were analyzed (GFP: $\lambda_{\text{max}}^{\text{abs}} = 488$ nm, $\lambda_{\text{max}}^{\text{em}} = 510$ nm). Single cells were gated by size (forward scattering height, FSC-H) and granularity (side scattering, SSC) with the associated device software. The single cell population was gated to detect GFP expressing cells to calculate the relative number of transfected cells. Transfection efficiency was determined by gating cells on forward scattering area (FSC-A) versus intensity area of the fluorescein isothiocyanate filter (FITC-A) as % GFP-positive cells.

Hemolysis Assay: The blood compatibility tests of the lipoplexes of OH4:DOPE were performed according the ISO 10993-4 guidelines. To evaluate the interactions of the lipoplexes with erythrocytes, erythrocytes were isolated from human blood of healthy donors, received from the Transfusion Medicine of the Medical Faculty of the Martin Luther University Halle-Wittenberg (2019-029). Before blood donation the voluntary donors gave written informed consent. For isolation of erythrocytes the fraction underneath the buffy coat was treated by size exclusion chromatography. To this end, a Biocoll solution (25 mL) was

overlaid with the erythrocyte fraction and mixed with heparin-containing PBS (30 + 30 mL) before. This mixture was centrifuged at 400 \times g for 30 min. Afterward, the supernatant was removed, and the resulting erythrocyte pellet was washed thrice with PBS buffer (pH 7.4) (30 mL; 2660 \times g; 7 min). Finally, the pellet was diluted with PBS (pH 7.4) to obtain an erythrocyte concentration of 8×10^9 cells mL⁻¹. The lipoplex dilutions (0.5 mL) were mixed with the erythrocyte solution (0.5 mL) and incubated for 1 h at 37 °C. Subsequently, the samples were centrifuged at 2300 \times g for 5 min and 100 μ L of the supernatant of each sample or control replicate were transferred to a well of a 96-well plate. The absorbance of the samples was measured at 540 nm with a plate reader (Spectrafluor, Tecan, Crailsheim, Germany). Various concentrations of the lipoplexes (depending on the amount of lipid) were tested (A_{sample}). As controls PBS buffer (pH 7.4) ($A_{\text{negative control}}$) or 1% Triton X-100 in PBS were used. Absorbance values of Triton X-100 were considered as 100% hemolysis ($A_{\text{positive control}}$). The samples and controls were tested in triplicates and the experiment repeated once. The percentage of free hemoglobin was calculated according to the following equation:

$$\text{Hemolysis} = \left[\frac{(A_{\text{sample}} - \text{blank}) - (A_{\text{negative control}} - \text{blank})}{(A_{\text{positive control}} - \text{blank})} \right] \times 100\% \quad (1)$$

The classification of the hemolytic activity was made according to ASTM F756–17 standard (Table 3):

Chorioallantoic Membrane Model: For the experiments, certified pathogen free fertilized chicken eggs were purchased from Valo BioMedia (Osterholz-Scharmbeck, Germany) and incubated at 37 °C with a relative humidity of >60% inside of a hatching incubator (Ehret KMB 6, Dipl. Ing. W. Ehret, Emmendingen, Germany). Chorioallantoic membrane model (CAM) experiments were performed as described previously.^[48] Three days after fertilization of the hens egg; EDD (egg development day) 3; a hole with a diameter of 3 mm was drilled into the basal part of the eggshell and approximately 3 mL of egg-white was removed from the egg. To expose the CAM, the apical part of the eggshell was sliced with a diameter of 30 mm. The hole was covered at the bottom end using cellophane tape and the apical part using a paraffin film to protect it from contamination. The eggs were incubated until 10 EDD, when 100 μ L of the lipoplex solution (containing 0.5 μ g GFP plasmid, either OH4:DOPE or Lipofectamine 2000) were injected into the mesoderm as triplicate (3 eggs per formulation). After injection the eggs were further incubated. 24 h after injection the CAM was cut out using a scalpel, washed with 0.9% NaCl and evaluated by confocal microscopy (LSM 700; Carl Zeiss) regarding GFP ($\lambda_{\text{max}}^{\text{abs}} = 488$ nm/ $\lambda_{\text{max}}^{\text{em}} = 510$ nm) fluorescence. For all of the acquisitions the same detector gain and settings of the spectral detection were used and every transfection experiment was repeated once.

Zebrafish Strains and Intravenous Injections: Zebrafish (*Danio rerio*, strain AB/TL) were maintained and handled according to the guidelines from the Zebrafish Model Organism Database (<http://zfin.org>) and in compliance with the directives of the local animal welfare committee of Leiden University. Fertilization was performed by natural spawning at the beginning of the light period, and eggs were raised at 28.5 °C in egg water (60 μ g mL⁻¹ Instant Ocean sea salts). The following previously established zebrafish lines were used Tg(*kdr*:GFP)^{s843},^[49] Tg(*kdr*:RFP-CAAX)^{s916},^[50] Tg(*mpeg*:GFP)^{gl22},^[51] Tg(*mpeg*:RFP-CAAX)^{ump2},^[52] and AB/TL wildtype. Lipoplex formulations were injected into 2 day old zebrafish embryos

Table 3: Hemolytic activity classification according to ASTM F756-17 standardization.

Hemolytic index above the negative control [%]	Hemolytic grade
0–2	Non-hemolytic
2–5	Slightly hemolytic
>5	Hemolytic

(52–56 hpf, hours post fertilization) using confocal microscopy as described previously.^[20] The following concentrations were injected: OH4:DOPE pDNA or mRNA lipoplexes (1 mg mL⁻¹) and Lipofectamine 2000 (0.9 mg mL⁻¹).

Zebrafish Imaging and Quantification: Biodistribution analysis of the lipoplexes was performed on 40× confocal z-stacks (with an optical thickness of 2 μm per slice). Laser intensity, gain, and offset settings were identical between stacks and sessions. Images were processed and quantified using the Fiji distribution of ImageJ.^[53]

In Vivo Transfection Studies in Mice: Investigation of in vivo transfection by lipoplexes was performed with 41–50 weeks old C57BL/6-Tyr^c Albino mice (B6N-Tyrc/BrdCrCl, Charles River Laboratories, USA) in a pilot study (two lipoplex treated mice and a control mouse). Animals were kept in individually ventilated cages (Type 2L; Tecniplast, Hohenpeißenberg, Germany) and provided access to water and mouse maintenance food (Ch.B.-63760735, rat and mouse maintenance food, sniff Spezialdiäten GmbH, D-59494 Soest, Germany) ad libitum. All animal procedures were approved by local ethics committee and are in accordance with the Austrian law for the protection of animals and the EU directive 2010/63/EU (approval number: 66.006/0027-WF/V/3b/2014).

Lipoplexes were prepared as described above but with slight changes needed for in vivo formulation. Lipoplexes were prepared at N/P ratio 4 by mixing cationic liposomes and reporter-plasmid to have the lipoplexes in 5% glucose (final concentration) as physiological medium. To track the in vivo transfection status of animals by bioluminescence imaging, reporter plasmid pCpG-hCMV-EF1a-LucSH coding for firefly luciferase gene was employed.^[40] Lipoplexes were injected intravenously into the lateral tail vein of mice at a dose of 2.5 mg of plasmid DNA per kg body weight. Mice were then imaged by bioluminescence imaging at 24 and 48 h after lipoplex administration. For bioluminescence imaging, mice were administered with D-Luciferin (120 mg kg⁻¹; subcutaneous injection) and bioluminescence signal collected by IVIS Spectrum CT Imaging System (Perkin Elmer Inc., Waltham, USA). During imaging, mice were anaesthetized with 2–2.5% isoflurane-oxygen mixture and mice shaved prior to imaging to improve the quality of bioluminescence signal. Thereafter, animals were euthanized and organs were imaged ex vivo by bioluminescence imaging. Image analysis was performed with Living Image software version 4.5.2.

Statistical Analysis: Data in the figures represent the mean of at least three independent experiments ± standard deviation. The related numbers of experiments is given as “n” in the caption. Statistical significance was determined by Mann–Whitney–Wilcoxon-test or one way ANOVA with Tukey's post-hoc test with a significance level α of 0.05; *p < 0.05.

Supporting Information

Supporting Information is available from the Wiley Online Library or from the author.

Acknowledgements

The authors thank S. Koch and C. Pilowski for technical assistance. Open access funding enabled and organized by Projekt DEAL.

Conflict of Interest

The authors declare no conflict of interest.

Data Availability Statement

The data that support the findings of this study are available from the corresponding author upon reasonable request.

Keywords

cationic lipids, ionizable lipids, lipid nanoparticles, mRNA-transfection, pDNA-transfection, zebrafish embryos

Received: December 14, 2021

Revised: February 10, 2022

Published online: March 30, 2022

- [1] C.-C. Ma, Z.-L. Wang, T. Xu, Z.-Y. He, Y.-Q. Wei, *Biotechnol. Adv.* **2020**, *40*, 107502.
- [2] a) B. L. Davidson, X. O. Breakefield, *Nat. Rev. Neurosci.* **2003**, *4*, 353; b) M. A. Kay, J. C. Glorioso, L. Naldini, *Nat. Med.* **2001**, *7*, 33; c) N. Nayerossadat, T. Maedeh, P. A. Ali, *Adv. Biomed. Res.* **2012**, *1*, 27; d) T. P. O'Connor, R. G. Crystal, *Nat. Rev. Genet.* **2006**, *7*, 261; e) Y. K. Sung, S. W. Kim, *Biomater. Res.* **2019**, *23*, 8.
- [3] a) A. Maitra, *Expert Rev. Mol. Diagn.* **2005**, *5*, 893; b) T. J. Levingstone, S. Herbay, J. Redmond, H. O. McCarthy, N. J. Dunne, *Nanomaterials* **2020**, *10*, 146; c) P. Zhang, E. Wagner, *Top. Curr. Chem.* **2017**, *375*, 26; d) A. L. Barnes, R. A. Wassel, F. Mondalek, K. Chen, K. J. Dormer, R. D. Kopke, *BioMagnetic Res. Technol.* **2007**, *5*, 1; e) W. Walther, I. Fichtner, P. M. Schlag, U. S. Stein, in *Gene Therapy of Cancer: Methods and Protocols*, (Eds.: W. Walther, U. S. Stein), Humana Press, Totowa, NJ **2009**, pp. 195.
- [4] a) I. Koltover, T. Salditt, J. O. Rädler, C. R. Safinya, *Science* **1998**, *281*, 78; b) J. O. Rädler, I. Koltover, T. Salditt, C. R. Safinya, *Science* **1997**, *275*, 810; c) P. R. Cullis, M. J. Hope, *Mol. Ther.* **2017**, *25*, 1467.
- [5] P. L. Felgner, T. R. Gadek, M. Holm, R. Roman, H. W. Chan, M. Wenz, J. P. Northrop, G. M. Ringold, M. Danielsen, *Proc. Natl. Acad. Sci. U. S. A.* **1987**, *84*, 7413.
- [6] a) K. K. Ewert, A. Zidovska, A. Ahmad, N. F. Bouxsein, H. M. Evans, C. S. McAllister, C. E. Samuel, C. R. Safinya in *Nucleic Acid Transfection*, (Eds.: W. Bielke, C. Erbacher), Springer Berlin Heidelberg, Berlin, Heidelberg **2010**, pp. 191; b) R. Koynova, B. Tenchov in *Nucleic Acid Transfection*, (Eds.: W. Bielke, C. Erbacher), Springer Berlin Heidelberg, Berlin, Heidelberg **2010**, pp. 51; c) I. S. Zuhorn, U. Bakowsky, E. Polushkin, W. H. Visser, M. C. Stuart, J. B. Engberts, D. Hoekstra, *Mol. Ther.* **2005**, *11*, 801.
- [7] a) A. Zidovska, H. M. Evans, K. K. Ewert, J. Quispe, B. Carragher, C. S. Potter, C. R. Safinya, *J. Phys. Chem. B* **2009**, *113*, 3694; b) K. Ewert, A. Ahmad, H. M. Evans, H.-W. Schmidt, C. R. Safinya, *J. Med. Chem.* **2002**, *45*, 5023.
- [8] a) S. Bhattacharya, A. Bajaj, *Chem. Commun.* **2009**, 4632; b) A. D. Miller, *Angew. Chem., Int. Ed.* **1998**, *37*, 1768.
- [9] C. Wölk, C. Janich, U. Bakowsky, A. Langner, G. Brezesinski, *Adv. Colloid Interface Sci.* **2017**, *248*, 20.
- [10] C. Wölk, S. Drescher, A. Meister, A. Blume, A. Langner, B. Dobner, *Chem. - Eur. J.* **2013**, *19*, 12824.
- [11] a) S. Tassler, D. Pawlowska, C. Janich, B. Dobner, C. Wölk, G. Brezesinski, *Phys. Chem. Chem. Phys.* **2018**, *20*, 6936; b) S. Tassler, D. Pawlowska, C. Janich, J. Giselbrecht, S. Drescher, A. Langner, C. Wölk, G. Brezesinski, *Phys. Chem. Chem. Phys.* **2018**, *20*, 17393.
- [12] R. G. W. Kirk, *Sci. Technol. Hum. Values* **2018**, *43*, 622.
- [13] D. Ribatti, *Mech. Dev.* **2016**, *141*, 70.
- [14] S. R. Pinnapireddy, J. Giselbrecht, B. Strehlow, C. Janich, C. Husteden, A. Meister, H. Loppnow, D. Sedding, F. Erdmann, G. Hause, G. Brezesinski, T. Groth, A. Langner, U. Bakowsky, C. Wölk, *Biomater. Sci.* **2020**, *8*, 232.
- [15] Y. Lei, M. Rahim, Q. Ng, T. Segura, *J. Controlled Release* **2011**, *153*, 255.
- [16] E. Baghdan, S. R. Pinnapireddy, B. Strehlow, K. H. Engelhardt, J. Schäfer, U. Bakowsky, *Int. J. Pharm.* **2018**, *535*, 473.

- [17] I. Tariq, S. R. Pinnapireddy, L. Duse, M. Y. Ali, S. Ali, M. U. Amin, N. Goergen, J. Jedelská, J. Schäfer, U. Bakowsky, *Eur. J. Pharm. Biopharm.* **2019**, 135, 72.
- [18] C. Husteden, F. Doberenz, N. Goergen, S. R. Pinnapireddy, C. Janich, A. Langner, F. Syrowatka, A. Repanas, F. Erdmann, J. Jedelská, U. Bakowsky, C. Wölk, T. Groth, *ACS Appl. Mater. Interfaces* **2020**, 12, 8963.
- [19] S. Sieber, P. Grossen, J. Bussmann, F. Campbell, A. Kros, D. Witzigmann, J. Huwyler, *Adv. Drug Delivery Rev.* **2019**, 151–152, 152.
- [20] F. Campbell, F. L. Bos, S. Sieber, G. Arias-Alpizar, B. E. Koch, J. Huwyler, A. Kros, J. Bussmann, *ACS Nano* **2018**, 12, 2138.
- [21] a) X. Zhou, F. Laroche, G. E. M. Lamers, V. Torracca, P. Voskamp, T. Lu, F. Chu, H. P. Spaink, J. P. Abrahams, Z. Liu, *Nano Res.* **2012**, 5, 703; b) C. Mauriello Jimenez, D. Aggad, J. G. Croissant, K. Tresfield, D. Laurencin, D. Berthomieu, N. Cubedo, M. Rossel, S. Alsaïari, D. H. Anjum, R. Sougrat, M. A. Roldan-Gutierrez, S. Richeter, E. Oliviero, L. Raehm, C. Charnay, X. Cattoën, S. Clément, M. W. C. Man, M. Maynadier, V. Chaleix, V. Sol, M. Garcia, M. Gary-Bobo, N. M. Khashab, N. Bettache, J.-O. Durand, *Adv. Funct. Mater.* **2018**, 28, 1800235; c) Z. Zhang, K. Wen, C. Zhang, L. Fabrice, Z. Wang, Q. Zhou, L. Zunfeng, J. P. Abrahams, Z. Xiang, *Front. Bioeng. Biotechnol.* **2020**, 8, 448; M. Cordeiro, L. Carvalho, J. Silva, L. Saúde, A. Fernandes, P. Baptista, *Nanomaterials* **2017**, 7, 10; e) J. Diao, H. Wang, N. Chang, X.-H. Zhou, X. Zhu, J. Wang, J.-W. Xiong, *Dev. Biol.* **2015**, 406, 196.
- [22] C. Patton, G. H. Farr, D. An, P. G. Martini, L. Maves, *Zebrafish* **2018**, 15, 217.
- [23] C. Janich, C. Wölk, S. Taßler, S. Drescher, A. Meister, G. Brezesinski, B. Dobner, A. Langner, *Eur. J. Lipid Sci. Technol.* **2014**, 116, 1184.
- [24] C. Janich, C. Wölk, F. Erdmann, T. Groth, G. Brezesinski, B. Dobner, A. Langner, *J. Controlled Release* **2015**, 220, 295.
- [25] C. Janich, S. R. Pinnapireddy, F. Erdmann, T. Groth, A. Langner, U. Bakowsky, C. Wölk, *Eur. J. Pharm. Biopharm.* **2017**, 118, 38.
- [26] C. Janich, D. Ivanusic, J. Giselsbrecht, E. Janich, S. R. Pinnapireddy, G. Hause, U. Bakowsky, A. Langner, C. Wölk, *Pharmaceutics* **2020**, 12, 805.
- [27] Z. u. Rehman, D. Hoekstra, I. S. Zuhorn, *ACS Nano* **2013**, 7, 3767.
- [28] M. Perez, A. Maiguy-Foinard, C. Barthélémy, B. Décaudin, P. Odou, *Pharm. Technol. Hosp. Pharm.* **2016**, 1, 91.
- [29] J. Giselsbrecht, C. Janich, S. R. Pinnapireddy, G. Hause, U. Bakowsky, C. Wölk, A. Langner, *Int. J. Pharm.* **2018**, 541, 81.
- [30] K. M. de La Harpe, P. P. Kondiah, Y. E. Choonara, T. Marimuthu, L. C. Du Toit, V. Pillay, *Cells* **2019**, 8, 1209.
- [31] V. E. Kerchberger, L. B. Ware, *Semin. Nephrol.* **2020**, 40, 148.
- [32] G. Chouinard-Pelletier, M. Leduc, D. Guay, S. Coulombe, R. L. Leask, E. A. V. Jones, *Biomed. Eng. Online* **2012**, 11, 67.
- [33] D. R. Brown, L. A. Samsa, L. Qian, J. Liu, J. Cardiovasc. Dev. Dis. **2016**, 3, 13.
- [34] M. Lundqvist, J. Stigler, G. Elia, I. Lynch, T. Cedervall, K. A. Dawson, *Proc. Natl. Acad. Sci. U. S. A.* **2008**, 105, 14265.
- [35] a) J. Rejman, G. Tavernier, N. Bavarsad, J. Demeester, S. C. de Smedt, *J. Controlled Release* **2010**, 147, 385; b) S. Zou, K. Scarfo, M. H. Nantz, J. G. Hecker, *Int. J. Pharm.* **2010**, 389, 232.
- [36] H. C. Yalcin, A. Amindari, J. T. Butcher, A. Althani, M. Yacoub, *Dev. Dyn.* **2017**, 246, 868.
- [37] a) S. E. Lindsey, P. G. Menon, W. J. Kowalski, A. Shekhar, H. C. Yalcin, N. Nishimura, C. B. Schaffer, J. T. Butcher, K. Pekkan, *Biomech. Model. Mechanobiol.* **2015**, 14, 735; b) J. Liu, M. Bressan, D. Hassel, J. Huisken, D. Staudt, K. Kikuchi, K. D. Poss, T. Mikawa, D. Y. R. Stainier, *Development* **2010**, 137, 3867.
- [38] S. Brunner, E. Fürtbauer, T. Sauer, M. Kurs, E. Wagner, *Mol. Ther.* **2002**, 5, 80.
- [39] N. Battista, D. Douglas, A. Lane, L. Samsa, J. Liu, L. Miller, *J. Cardiovasc. Dev. Dis.* **2019**, 6, 6.
- [40] G. Navarro, G. Maiwald, R. Haase, A. L. Rogach, E. Wagner, C. T. de Ilarduya, M. Ogris, *J. Controlled Release* **2010**, 146, 99.
- [41] B. Su, A. Cengizoglu, K. Farkasova, J. R. Viola, M. Anton, J. W. Ellwart, R. Haase, E. Wagner, M. Ogris, *Mol. Ther.* **2013**, 21, 300.
- [42] a) D. Simberg, A. Weiss, Y. Barenholz, *Hum. Gene Ther.* **2005**, 16, 1087; b) F. Sakurai, T. Nishioka, F. Yamashita, Y. Takakura, M. Hashida, *Eur. J. Pharm. Biopharm.* **2001**, 52, 165.
- [43] a) M. Ogris, A. K. Kotha, N. Tietze, E. Wagner, F. S. Palumbo, G. Giammona, G. Cavallaro, *Pharm. Res.* **2007**, 24, 2213; b) S. Loisel, C. Le Gall, L. Doucet, C. Ferec, V. Floch, *Hum. Gene Ther.* **2001**, 12, 685.
- [44] H. Zhang, J. Bussmann, F. H. Huhnke, J. Devoldere, A.-K. Minnaert, W. Jiskoot, F. Serwane, J. Spatz, M. Röding, S. C. de Smedt, K. Braeckmans, K. Remaut, *Adv. Sci.* **2022**, 9, 2102072.
- [45] Q. Cheng, T. Wei, L. Farbiak, L. T. Johnson, S. A. Dilliard, D. J. Siegwart, *Nat. Nanotechnol.* **2020**, 15, 313.
- [46] T. Walker, I. Müller, C. Raabe, B. Nohe, C. Zanke, G. Ziemer, H.-P. Wendel, *Eur. J. Cardiothorac. Surg.* **2011**, 40, 1241.
- [47] A. Huertas, C. Guignabert, J. A. Barberà, P. Bartsch, J. Bhattacharya, S. Bhattacharya, M. R. Bonsignore, L. Dewachter, A. T. Dinh-Xuan, P. Dorfmueller, M. T. Gladwin, M. Humbert, T. Kotsimbos, T. Vassilakopoulos, O. Sanchez, L. Savale, U. Testa, M. R. Wilkins, *Eur. Respir. J.* **2018**, 51, 1700745.
- [48] A. Özçetin, A. Aigner, U. Bakowsky, *Eur. J. Pharm. Biopharm.* **2013**, 85, 711.
- [49] S.-W. Jin, D. Beis, T. Mitchell, J.-N. Chen, D. Y. R. Stainier, *Development* **2005**, 132, 5199.
- [50] B. M. Hogan, F. L. Bos, J. Bussmann, M. Witte, N. C. Chi, H. J. Duckers, S. Schulte-Merker, *Nat. Genet.* **2009**, 41, 396.
- [51] F. Ellett, L. Pase, J. W. Hayman, A. Andrianopoulos, G. J. Lieschke, *Blood* **2011**, 117, e49.
- [52] M. Nguyen-Chi, Q. T. Phan, C. Gonzalez, J.-F. Dubremetz, J.-P. Levrard, G. Lutfalla, *Dis. Model. Mech.* **2014**, 7, 871.
- [53] a) J. Schindelin, I. Arganda-Carreras, E. Frise, V. Kaynig, M. Longair, T. Pietzsch, S. Preibisch, C. Rueden, S. Saalfeld, B. Schmid, J. Tinevez, D. J. White, V. Hartenstein, K. Eliceiri, P. Tomancak, A. Cardona, *Nat. Methods* **2012**, 9, 676; b) C. A. Schneider, W. S. Rasband, K. W. Eliceiri, *Nat. Methods* **2012**, 9, 671.